Chapter 2

X-Ray Diffraction Analysis of Structural Changes Induced by Overrolling

Oskar Beer

Additional information is available at the end of the chapter

http://dx.doi.org/10.5772/intechopen.74251

Abstract

A new method of X-ray diffraction analysis to evaluate structural changes in rolling element bearing components is demonstrated. The basics of residual stress measurement by X-ray diffraction based on the $\sin^2\psi$ method are explained. Microstructural analysis is performed on bearing components after rig testing and after use in field. The results shown in this chapter are mostly derived from rolling element bearing applications in aero engines. First it is shown how an estimation of a rolling contact fatigue life can be derived from microstructural analysis. Second it will be shown that surface near induced residual stresses can improve rolling contact fatigue life. Finally it will be demonstrated that basic results from rig testing can be transferred to use in field.

Keywords: X-ray diffraction, structural changes, residual stress, rolling contact fatigue life, stress limit

1. Introduction

X-ray analysis enables the detection of structural changes in materials. By performing this kind of analysis on rolling element bearing components after use structural changes caused by the overrolling process can be analyzed. This analysis enables the possibility to get data for stress limits and to compare rig testing results and field experience. In many cases it is more effective to get such data by X-ray analysis than by statistic evaluation of rig testing. A comparison of data from rig testing with data from field experience is often only possible by X-ray analysis of parts coming from use in field. Several work has already be done in this field [1–5]. The method of analysis presented here also uses data from residual stress analysis, especially the full width at half maximum value, also called peak width for the estimation of life data for

rolling element bearings. The focus of evaluation here is mainly on mainshaft bearing applications in aero engines, therefore the material analyzed is the high speed steel M50. The basics of X-ray analysis of residual stresses are presented, then some information about stresses due to rolling contact is given. Several samples of X-ray analysis performed on parts from rig testing and from use in field show the possibilities of this kind of evaluation.

2. X-ray residual stress analysis

2.1. Principle of measurement

By elastic deformation the distances within the unit cells of a crystallic material become smaller in case of compressive stress or larger in case of tensile stress respectively. **Figure 1** shows schematically the variation of a lattice distance due to tensile stresses. The positions of the atoms are represented by small circles. The distance d′ of the atoms due to the tensile stress σ is larger than the distance d of the unloaded condition. The elongation of the lattice in direction of the stress σ is accompanied by a shortening perpendicular to the direction of σ. The ratio between the elongation in direction of the stress σ and the shortening perpendicular is called Poisson's ratio ν. The elongation due to elastic loading by the tension σ can be calculated by Hook's law with the modulus of elasticity E as characteristic parameter. X-ray diffraction analysis makes possible the determination of variations in interatomic distances and hence enables the calculation of macroscopic stresses.

2.2. Bragg's law

When a beam of X-ray falls on a specimen, the X-ray photons interact with the electrons of the target and scattering occurs. X-ray diffraction analysis is based on the scattering with no energy loss, the scattered radiation will retain the same wavelength as the incident beam. When two or more waves trains propagate at the same location into the same direction, they interfere which is a kind of superposition of one wave upon the other. If wave trains are in phase, they add to another, if they are exactly out of phase, they annihilate each other. **Figure 2** illustrates the geometric condition of reinforcement on a schematic lattice. Scattering points are the atoms of the

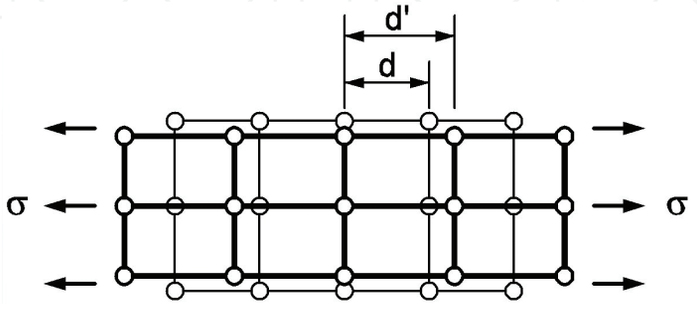

Figure 1. Shift of the unit cell dimensions due to a tensile stress σ. d: lattice plane distance without stress; and d′: lattice plane distance due to the stress σ.

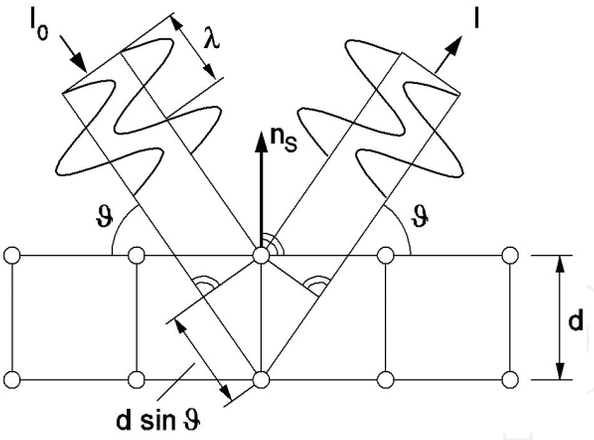

Figure 2. Diffraction of x-radiation at a crystal lattice.

lattice. Reinforcement will occur, when the difference in the path lengths of the two interfering waves is equal to an integer multiple of the wavelength, the equation for this is given in Eq. (1) which is the statement of Bragg's law.

Bragg's law for constructive interference:

$$n\lambda = 2d\sin\vartheta \ (n = 1, 2, 3\ldots) \tag{1}$$

Only if the incident angle ϑ fits to Bragg's law, diffraction maybe observed at the emergent beam at the same angel ϑ.

By known wavelength λ and measured diffraction angle ϑ the lattice plane distance d can be calculated:

$$d = n\lambda/2\sin\vartheta \tag{2}$$

The intensity of the diffracted beam around the Bragg angle ϑ_B is shown schematically in **Figure 3**. The peak can be characterized by the peak position ϑ_B and the peak width. The peak position correlates width the lattice plane distance d and by this with the material stress σ. The peak width correlates with the density of dislocations beside other microstructural properties and therefore it is correlated to a certain extent with the strength of the material.

2.3. The ψ angle

The penetration depth of the X-radiation typically used for diffraction analysis is only a few micrometers in most metals. This means that only the surface near region is used for the measurement. Material stresses act predominately parallel to the surface of a part, especially close to a surface no stress component perpendicular to this surface is possible (due to the balance of forces). The determination of material stresses by a variation of lattice distance d according to **Figure 2** takes place perpendicular to the surface. This means, that lattice planes easy to be measured (parallel to the surface) have no direct correlation to the acting material

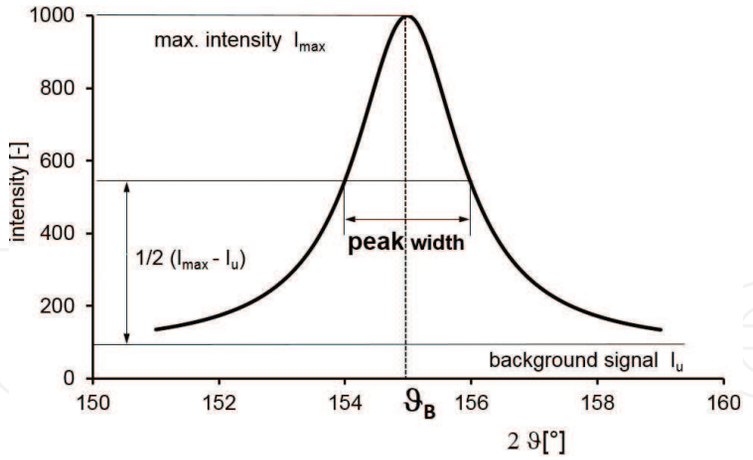

Figure 3. Intensity of the diffracted beam around the Bragg angle ϑ_B (schematic).

stress, diffraction from lattice planes having the highest correlation to the acting stress (perpendicular to the surface) are absorbed and cannot be measured. The way to overcome this problem is a measurement at an inclination angle, called tilt angel ψ to the normal of the plane of the surface. **Figure 4** shows this principle.

A measurement according to **Figure 4** is only possible when in the irradiated area enough lattice planes perpendicular to the adjusted tilt angle ψ are available. Metallic materials, especially construction materials, consist of an arrangement of small crystals, called grains. The orientation of these grains is in many cases randomly distributed (if there is a preferred orientation of the grains due to the manufacturing process, called texture, e.g. due to intensive rolling, the method described here is not applicable at this fashion). **Figure 5** shows schematic grains with different orientation at the surface of a part. The average size of the grains in many construction materials is small compared to the irradiated area (e.g. the average grain size in steels is app. 60–20 μm, the diameter of the irradiated area is typically 1–4 mm), therefore enough grains with an orientation according to the adjusted tilt angle are available and a measurement is possible.

The principle of an experimental setup for performing residual stress measurements is shown in **Figure 6a**, a photograph of the device used for the following investigations is shown in **Figure 6b**. The X-rays used in diffraction analysis are produced by an evacuated tube. The target (anode) is water cooled, the target material for residual stress analysis at steel is typically chromium. The radiation emitted consists of a continuous spectrum, called bremsstrahlung, with some superimposed narrow spikes. One of these spikes, the Kα spike, is used for diffraction analysis, all the other radiation is absorbed by filters (for the use of Eq. (2) a nearly monochromatic X-radiation is necessary). For detection of the irradiated X-rays today mainly position sensitive solid state detectors are used. These detectors allow the analysis of the complete diffracted beam around the Bragg angle.

The direction of the normal and shear stress components measured by ψ-variation is perpendicular to the rotation axis for the ψ-tilts.

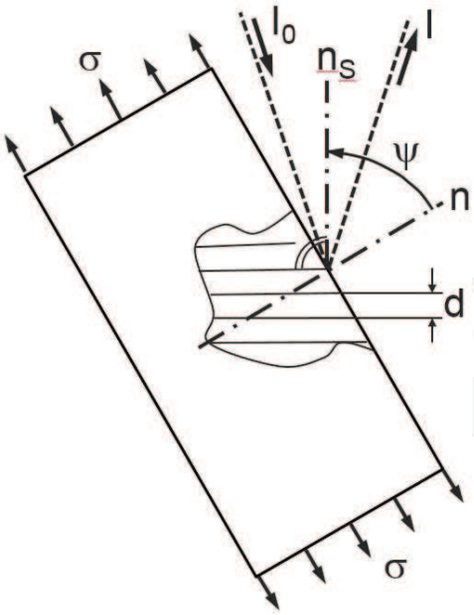

Figure 4. Diffraction at a tilt angle ψ.

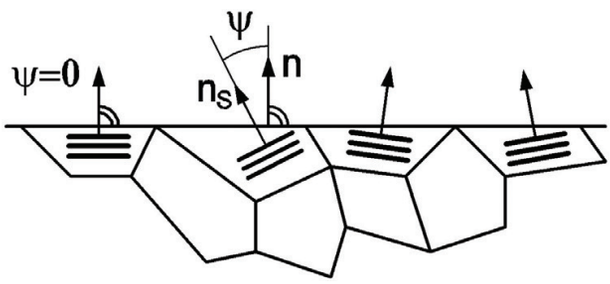

Figure 5. Orientation of grains at the surface (schematic). n: normal to the surface, n_s: normal to the lattice, and ψ: tilt angle.

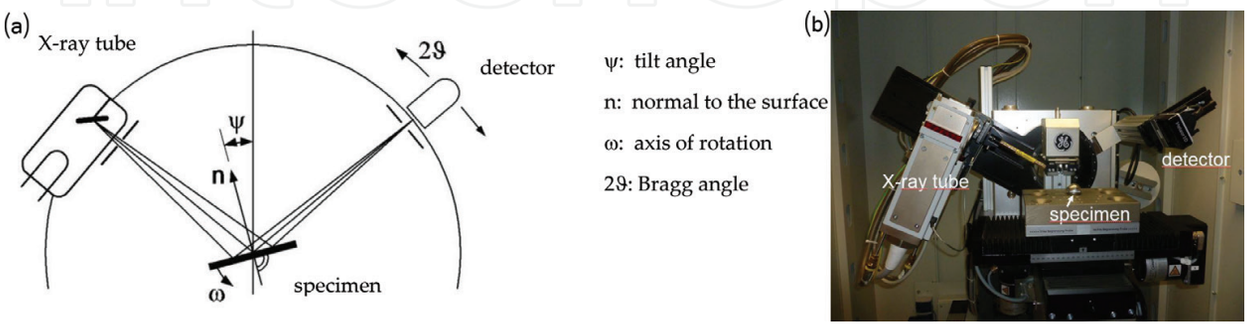

Figure 6. a: Schematic of an X-ray diffractometer, ω mode. b: Photograph of the device used for X-ray stress analysis.

2.4. The $\sin^2\psi$ chart

The following relation applies to describe the dependence of the lattice plane distances from the acting stress [6, 7]:

$$(d\psi - d_0)/d_0 = \tfrac{1}{2}\, s_2 \left[\sigma \sin^2\psi + \tau \sin 2\psi\right] + c \tag{3}$$

where $d\psi$ is the lattice plane distances of the planes with a tilt angle ψ in relation to the surface, d_0 is the lattice plane distances of a stress free crystal, s_2 is the X-ray elastic constant, material property to be known, σ is the normal stress acting parallel to the surface, and τ is the shear stress.

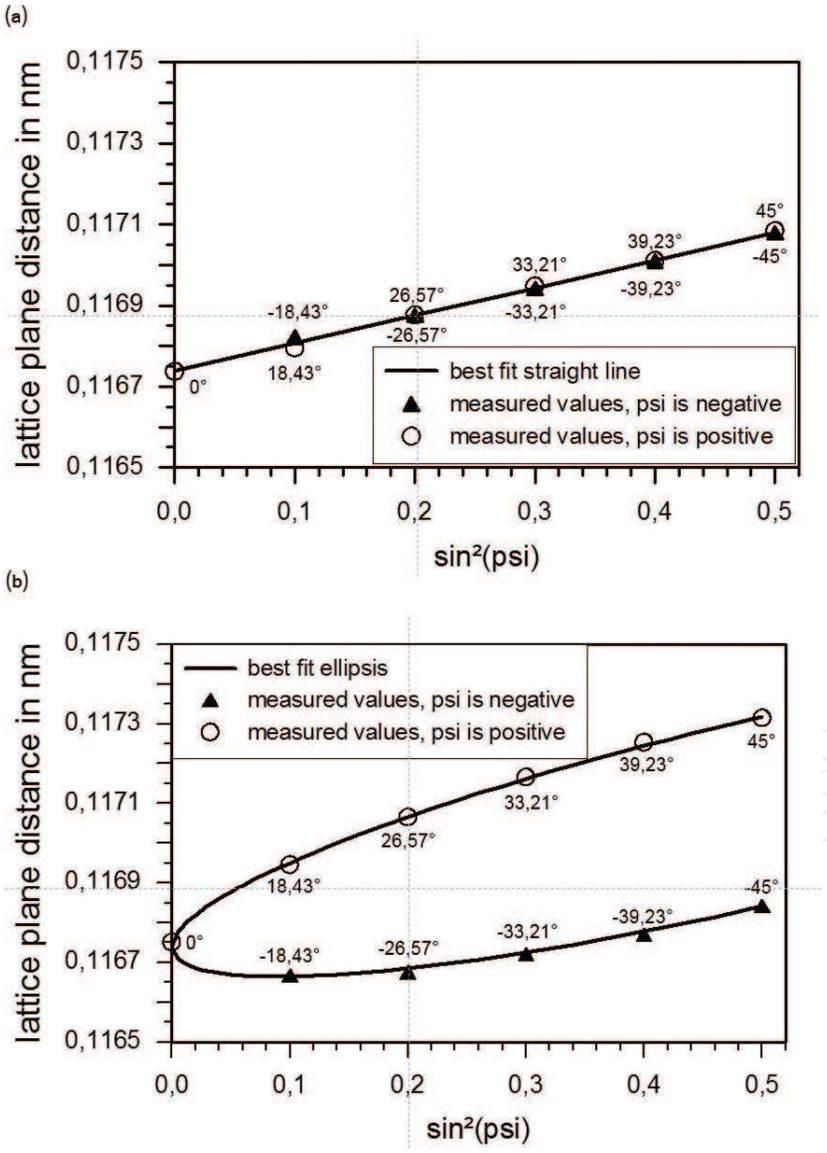

Figure 7. a: Example of a $\sin^2\psi$ chart without shear stress: straight line. b: Example of a $\sin^2\psi$ chart with shear stress: ellipsis.

http://dx.doi.org/10.5772/intechopen.74251

There are three unknown values in the $\sin^2\psi$ formula (3), σ, τ and c. These values could be determined by the measurements of the lattice plane distances $d\psi$ for three different ψ-angles. For a lower uncertainty in the final values, the measurement of the lattice plane distances $d\psi$ should be performed for more than three ψ-angles. If no shear stress t is present, the $\sin^2\psi$ formula (3) requires a straight line as a result of a plot of $d\psi$ against $\sin^2\psi$. If the shear stress τ is not negligible, the term $\tau \sin 2\psi$ transforms the straight line into an ellipsis. The slope of its big main axis is determined by σ, its width by τ. **Figure 7a** shows a $\sin^2\psi$ chart with no shear stress present, **Figure 7b** shows a $\sin^2\psi$ chart for a steel where shear stress is present.

3. Stresses due to rolling contact

The contact stresses arising from the contact between two elastic solids can be calculated by the Hertzian equations (with some assumptions: pure elastic material, dimensions of the solids are big compared with the contact area, frictionless contact, these assumptions are nearly fulfilled in rolling element bearing applications). In case of microstructural changes, the material behavior in the zone of maximum stress is not purely elastic. Nevertheless the Hertzian analysis can still be used to rationalize the observed damage accumulation. The stress field inside the bodies is characterized by a triaxial stress state, comprising the three principal stress components. In order to express the material stress beneath the contact zone and allow a comparison with the uniaxial yield strength, an equivalent stress can be calculated. The von Mises equivalent stress σ_{vgl} agrees best with many experimental results and is mostly used. An alternative is to calculate the maximum shear stress 2τ according to Tresca, which leads to results nearly the same or equivalent to von Mises equivalent stress (depending on the

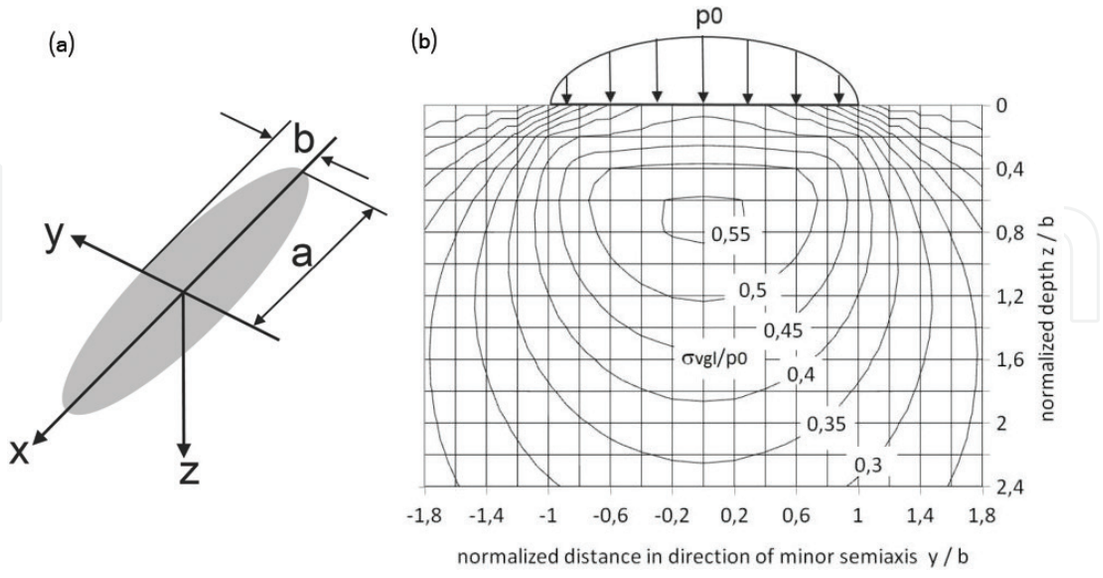

Figure 8. (a) Contact surface typical for a ball bearing, ellipsis, a: major semiaxis, b: minor semiaxis, y direction of overrolling. (b) Contour plot of the von Mises equivalent stress σ_{vgl} under the contact surface along the direction of overrolling (y direction according to **Figure 8a**). The stress is normalized to the Hertzian pressure p0, distances are normalized to the minor semiaxis of the contact ellipse b (a/b = 20).

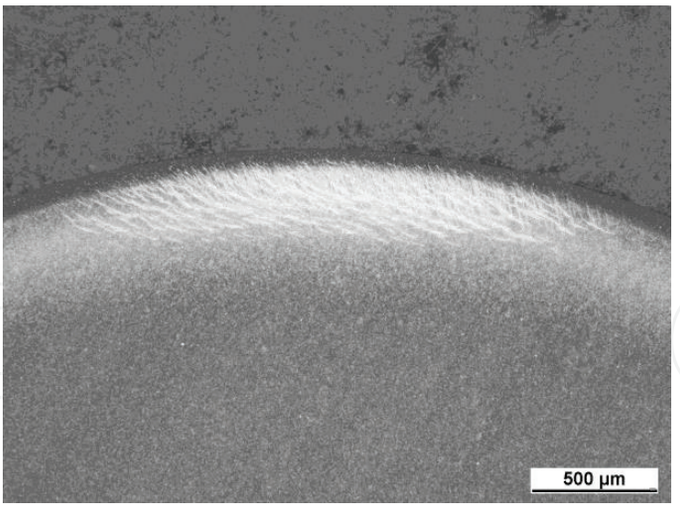

Figure 9. Micrograph showing microstructural changes below the surface of a ball (section perpendicular to the rolling track), after testing for 100 h at a Hertzian pressure of 3000 MPa, many white bands ("white ribbons") are visible in the subsurface zone.

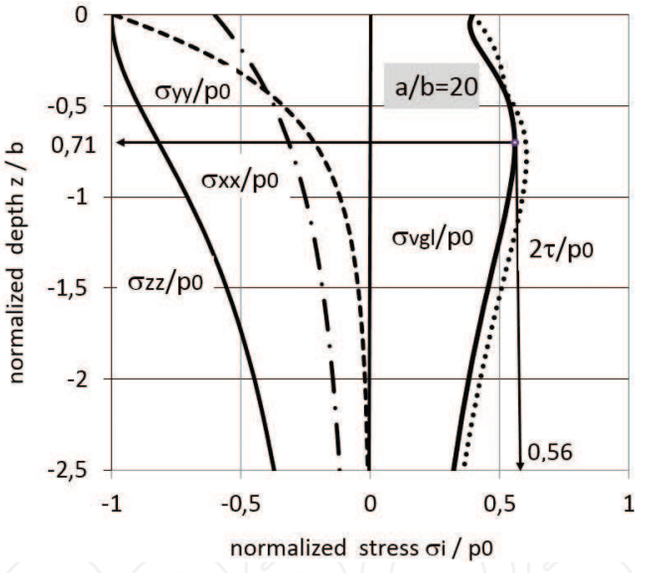

Figure 10. Stress distribution below the raceway surface (away from the axis of contact) for a Hertzian contact (a/b = 20), stress parameters are normalized to the Hertzian pressure p0, the depth coordinate is normalized to the minor semiaxis of the contact ellipse b.

stress components) and is simpler in several applications (in case of a principal state of stress). **Figure 8a** shows a contact area typical for a contact in a ball bearing, **Figure 8b** a contour plot of the von Mises equivalent stress σ_{vgl} under the contact surface. The maximum pressure occurs in the center of the contact surface and is called Hertzian pressure. Below the contact area a complex stress state develops. A micrograph taken in the subsurface zone of a bearing ring after intensive overrolling shows microstructural changes, "white ribbons" in about the depth of the maximum equivalent stress, see **Figure 9**. **Figure 10** shows the course of the three principal stress components along the axis of contact (z-axis) and the von Mises equivalent stress together with the max. shear stress (Tresca) for an elongated contact ellipse [2].

Away from the axis of contact the principal axes of the stress at a given position are not longer aligned with the sample coordinate system.

4. Analysis of bearing components

4.1. Details of the performed analysis

All analysis of the investigated components was done by position dispersive, monochromatic X-ray diffraction using a conventional diffractometer operated in iso-inclination. More sophisticated methods like the use of a synchrotron as X-ray source or the application of neutron diffraction was not necessary to achieve the pursued goals. The X-ray diffraction analysis was performed according to common standards (EN 13925, EN15305), Cr-Kα radiation was used, LPA (**L**orenz/**P**olarization/**A**bsorption)-correction was applied. The stress component parallel to the surface in direction of overrolling was measured. Depth profiles of residual stress and peak width were measured by a successive local electro chemical removal of surface layers. This procedure is necessary because the penetration depth of the Cr-Kα radiation in steel is only a few micrometers and a mechanical removal of material would create additional residual stresses. No correction of the stress redistribution due to the material removal was applied.

Comprehensive work in this field has already be done [1–5], here the evaluation is based more on the peak width and the analyzed material is the high speed steel M50.

4.2. Bearing steel M50

M50 is a high speed steel which exhibits high hardness and high compressive strength also at elevated temperatures. The chemical composition is (weight-percent):

0.85 % C/4.1 % Cr/4.2 % Mo/1 % V.

M50 is widely used for aeroengine bearings (VIMVAR quality corresponding to AMS 6491). The heat treating comprises an austenitizing at a temperature of approximately 1100°C, quenching in salt or in pressurized nitrogen gas and tempered several times at temperature of around 540°C. The resulting hardness is typically in the range of 61–64 HRC, the content of retained austenite is usually below 3%.

4.3. Experimental setup

The test rig used for performing overrolling tests is the so called "single ball test rig". The principle of this test rig is shown in **Figure 11**. The test component is a ball which rolls between two rings having curved races. One ring is driven by a motor, the load is applied by a hydraulic system. The ball is fixed by a retainer such that the overrolling of the ball occurs along in one rolling track. The lubrication of the contact zone is done by oil jets, the inlet temperature is approximately 140°C in order to be comparable to an application in an aeroengine, more details about rig testing can be found in [2].

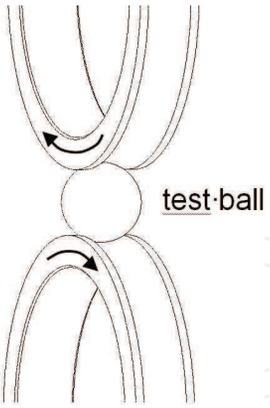

Figure 11. Schematic of the single ball test rig, ball diameter is app. 20–40 mm, speed of the rings is typically 7500 min^{-1}, race diameter of the rings is 175 mm.

The procedure to get structural changes is to run the single ball test rig with several balls for a fixed time (before visible failure) at different levels of pressure. Afterwards an X-ray based evaluation is performed on these balls. **Figure 12** shows calculated profiles of von Mises equivalent stress under the contact surface of a ball in the single ball test rig.

4.4. Evaluation results

4.4.1. Estimation of rolling contact fatigue life

Single ball rig tests were performed at different contact pressures. **Figure 13a** and **b** shows depth profiles of measured residual stress and peak width (see also **Figure 3**) after 100 h test run at Hertzian pressures of 1900 and 3000 MPa, respectively. The difference in peak width before and after testing, called "integral change in peak width," can be used to obtain an estimate of the endurance limit, see also [2, 3]. **Figure 14** shows the principle of the evaluation of the integral change in peak width. By plotting the so evaluated integral change in peak width

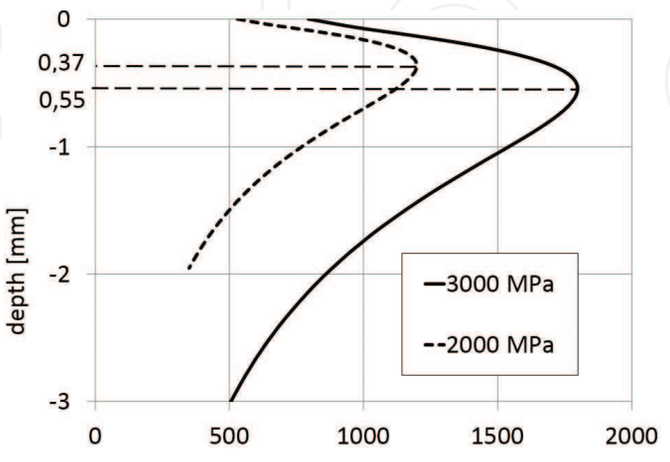

Figure 12. Calculated von Mises equivalent stress below the raceway for a ball (diameter 41 mm) in the single ball test rig at two different levels of Hertzian pressure.

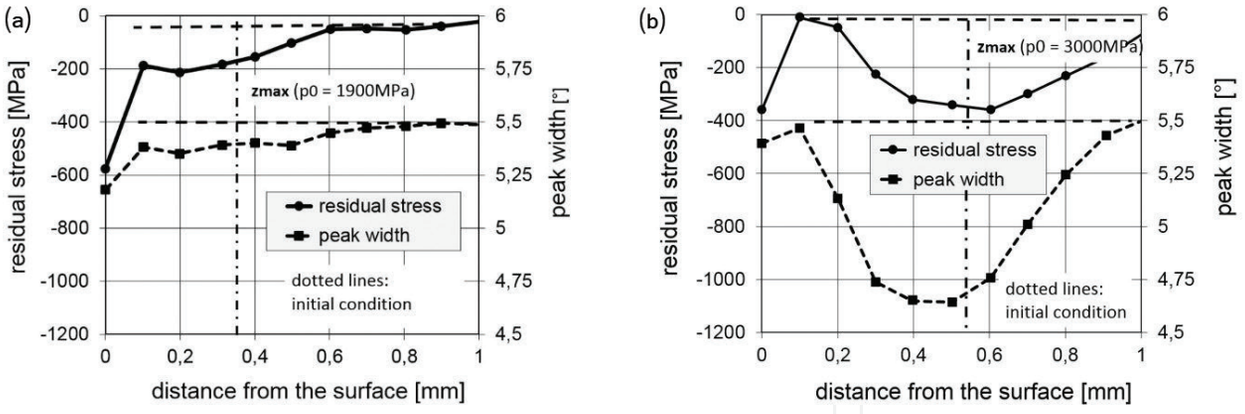

Figure 13. Measured distribution of residual stress (solid line) and peak width (dotted line) below the raceway surface in M50 balls after 100 h test in single ball test rig at a Hertzian pressure of (a) 1900 MPa and (b) 3000 MPa respectively, at an oil temperature of 140°C, zmax: calculated depth of maximum von Mises equivalent stress.

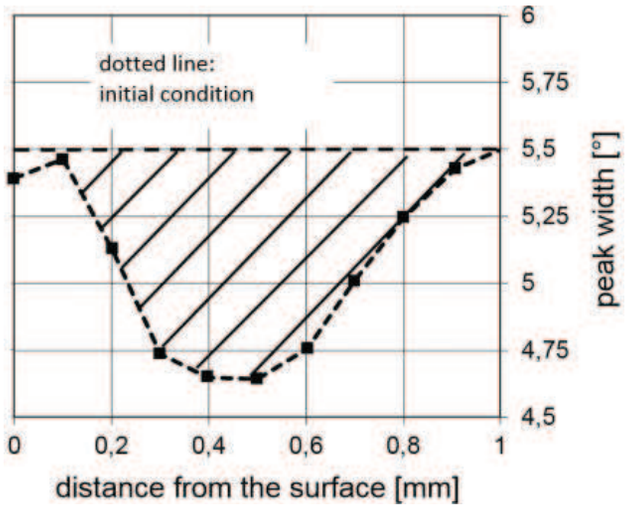

Figure 14. Distribution of peak width according to **Figure 13b**. Hatched area: integral change in peak width.

versus the applied maximum Hertzian contact pressures and fitting a straight line through these data points, an endurance limit in terms of an allowed maximum contact pressure (below which no fatigue damage will be accumulated) can be determined by extrapolation to zero peak width change. This procedure is shown in **Figure 15**. The estimated value for the endurance limit S0 of app. 1800 MPa according to **Figure 15** agrees well with experience from comprehensive testing and field experience.

4.4.2. Influence of residual compressive stresses

Residual stresses caused by heat treating (e.g. case hardening, nitriding) or mechanical induced residual stresses mostly act in directions parallel to the surface (in x- and y-direction according to the set of axis used here, see also **Figure 8a**). Residual stresses in the material will be superimposed on the stresses induced by the contact between the rolling element and the raceway surface and may then influence the equivalent stress [2, 3, 8, 9]. As residual stresses

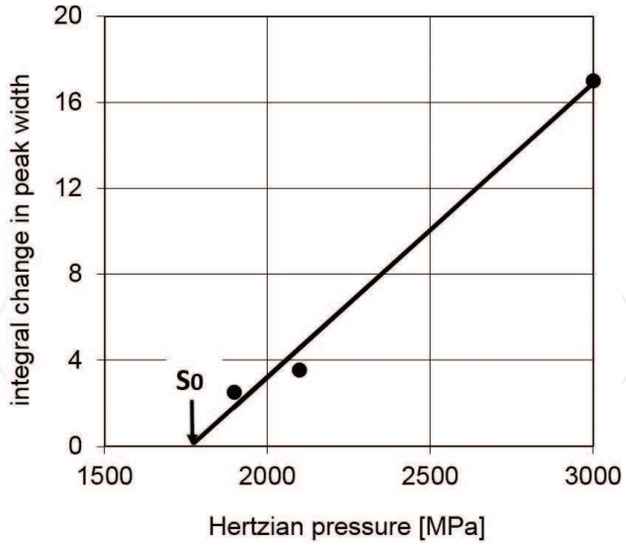

Figure 15. Estimation of an endurance limit S0 in terms of an allowed maximum contact pressure (oil temperature 140°C), y-axis arbitrary units.

typically act predominately in x- and y-direction, a shift of the principal stresses in x- and y-direction occurs whereas the principal stress in z-direction is less influenced. Compressive residual stresses (in a certain range) typically result in a reduction of the equivalent stress level. **Figure 16** shows the influence of compressive residual stresses on the von Mises equivalent stress in case of an axisymmetric contact (ball-ball).

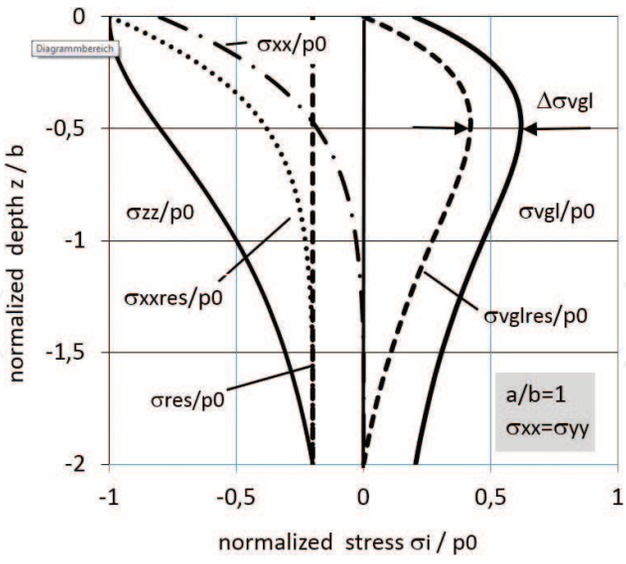

Figure 16. Stress distribution below the raceway surface for a Hertzian point contact (a/b = 1, $\sigma_{xx} = \sigma_{yy}$) without (solid curves) and with (dashed curves) compressive residual stress (the residual stress profile σ_{res} is here simplified as a constant compressive). The von Mises equivalent stress without consideration of residual stress (solid line) and with consideration of residual stress (dashed line), resulting in a reduction in the equivalent stress $\Delta\sigma_{vgl}$. The stress parameters are normalized to the Hertzian pressure p0, the depth coordinate is normalized to the radius of the contact surface.

By performing the single ball test procedure with balls which were tumbled (also called scoured in case of an intensive tumbling) after heat treating to induce compressive residual stresses the beneficial influence of compressive residual stresses on the overrolling performance can be shown. **Figure 17** shows residual stress and peak width distributions of tumbled balls after testing at two different contact pressure levels. **Figure 18** shows the evaluation of the endurance limit for both tumbled and not tumbled balls. As can be seen, the evaluated endurance limit of the tumbled balls is significantly higher.

The evaluation of several balls exposed to rolling contact fatigue in rig testing showed the following results:

- There seems to exist a stress (or maximum contact pressure) limit for the development of structural changes.
- Compressive residual stresses can raise the stress limit for the development of structural changes.

In rig testing the test conditions are well known and typically are maintained constant during the whole test run. In field use the operating conditions (load, temperature, etc.) are mostly not constant and not fully known. An evaluation of bearings after field use by X-ray methods offers the possibility to compare the test results with results from use in the field.

4.5. Field experience

Unlike as many rig tests, the load during a flight cycle is not constant. Maximum load typically occurs during take-off, while during normal flight conditions the load generally is lower. Also, different and variable temperatures and vibrations occur during the different parts of the flight cycle. Therefore, structural changes after field use are the result of a more or less periodic and complex load history. Since the full load history of an aero engine bearing as well

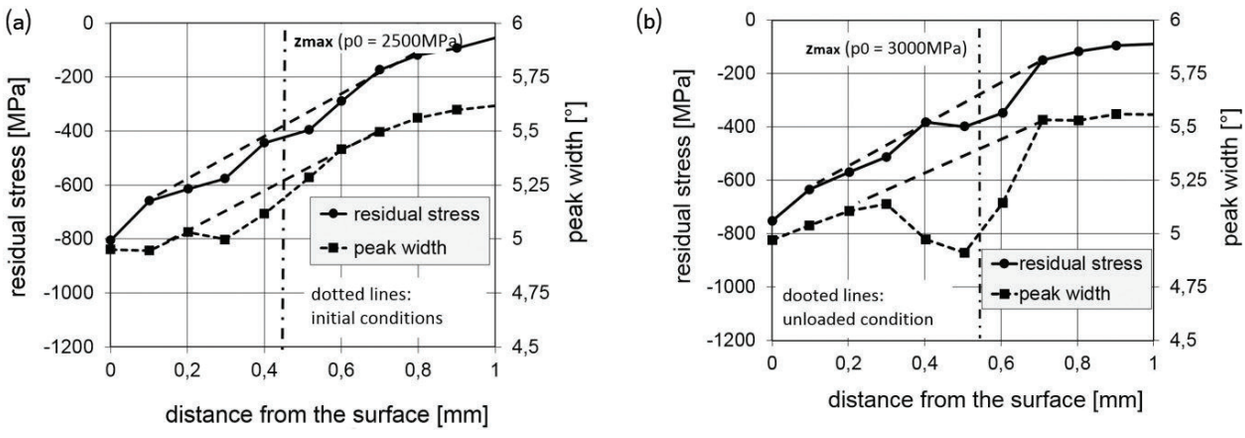

Figure 17. Measured distribution of residual stress and peak width below the raceway surface in tumbled M50 balls after 100 h test in the single ball test rig at the Hertzian pressure: (a) 2500 MPa and (b) 3000 MPa respectively, at an oil temperature of 140°C, z_{max}: calculated depth of maximum equivalent stress.

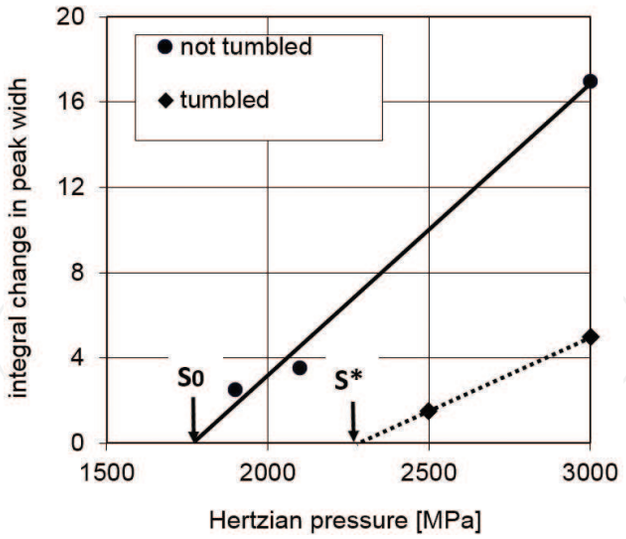

Figure 18. Estimated endurance limits in terms of allowed maximum contact pressure (below which no fatigue damage will be accumulated). S* of tumbled and S_0 of not tumbled M50 balls (oil in temp. 140°C), y axis arbitrary units.

as its temperature, vibration level etc. are not fully known, a direct comparison between rig test results and evaluation results from use in the field is not fully possible. However, based on the techniques discussed here, general experiences from laboratory testing can still, as will be shown, successfully transferred to field applications, see also [2].

The following evaluation results are taken from bearing parts after considerably time in field use. Two measures are handled for the characterization of the duration in field use:

TSN: Time Since New [h]

CSN: Cycles Since New.

4.5.1. Limit stress for structural changes

In order to check whether a stress limit for microstructural changes exists for field use, an inner ring of an used roller bearing was investigated. The stress acting in the subsurface zone of roller bearings are generally lower than for ball bearings, therefore even after long time in field use, no structural changes are expected. **Figure 19** shows measured distribution of residual stress and peak width for the inner ring of a roller bearing from a V2500 aero engine after TSN 37,380 h. This bearing did not show any indication of spalling or wear. The X-ray evaluation shows no indication of any structural changes. Although the stress history is not fully known in detail, the absence of any indication of structural changes suggests, that also in field use for a long time, a limit stress for structural changes may exist.

4.5.2. Influence of residual stress

A possibility of investigation the influence of residual stresses on the formation of structural changes in field use was given in case of a ball bearing of a GE90 aero engine with a TSN of 20,492 h. The rings and the balls were made from M50, while the balls were additionally tumbled to induce compressive residual stresses. This bearing showed slight indications of

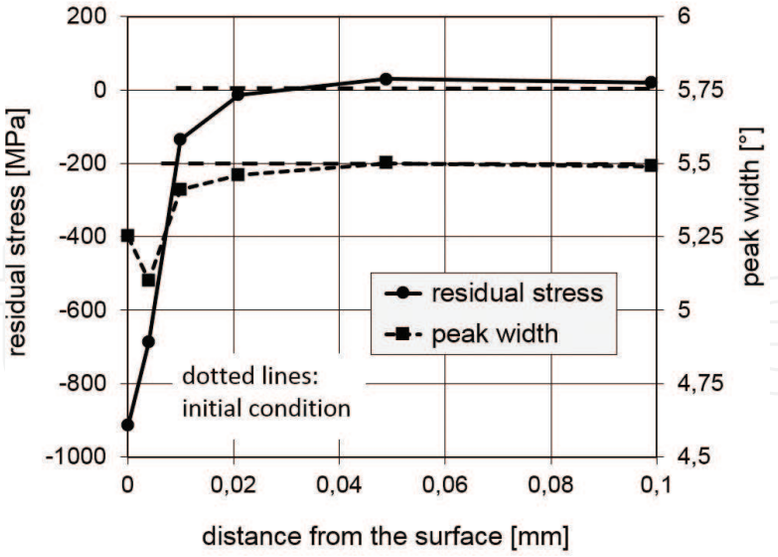

Figure 19. Measured distribution of residual stress and peak width below the raceway surface in a roller bearing inner ring, TSN 37,380 h, there are no indications of structural changes (only the typical peaks close to the surface due to hard machining), the Hertzian pressure is assumed to be at most 1200 MPa.

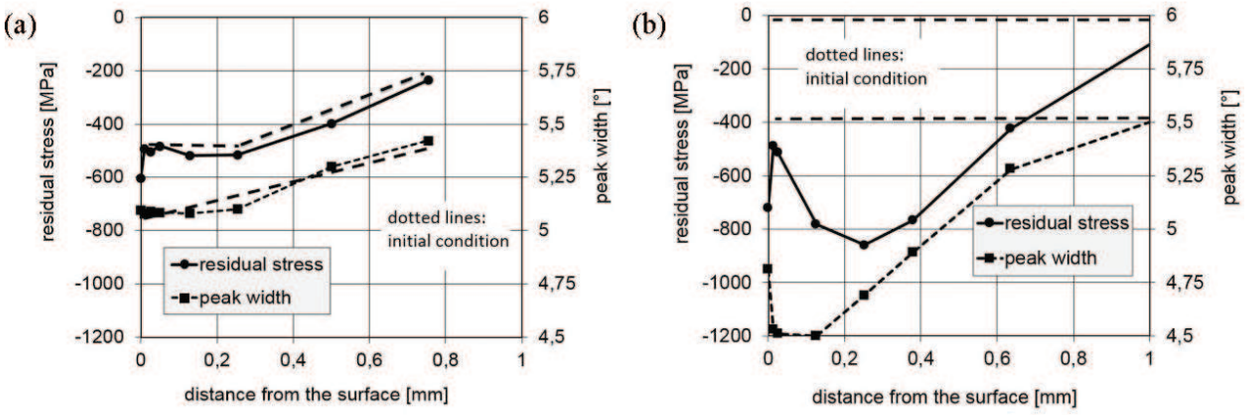

Figure 20. Measured distribution of residual stress and peak with from components of a GE90 aero engine, TSN 20,492 h (a) below the surface in a ball (tumbled) showing no indication of structural changes and (b) below the raceway surface in an inner ring, showing marked difference between the initial condition and the condition after use in field, suggesting considerably microstructural changes. Hertzian pressure assumed to be maximum 2000 MPa.

spalling on all components and was therefore taken out of service. **Figure 20** shows the measured distribution of residual stress and peak width versus the depth below the raceways, for a ball and an inner ring, respectively.

5. Conclusions

The microstructural evaluation of bearing components after rig testing shows that induced surface-near compressive residual stresses can improve the rolling contact fatigue life. It is further possible to derive approximate values for the endurance limit using X-ray based

microstructural analysis. A comparison of microstructural evaluation results on components taken from engine bearings after use in the field with results from parts after rig testing shows, that basic causes and effects are similar in both cases. These results therefore provide a confirmation that results from rig testing can be used for bearing design also in demanding applications.

Acknowledgements

The author acknowledges the technical support of Dr. Böhmer.

Author details

Oskar Beer

Address all correspondence to: oskar.beer@schaeffler.com

FAG Aerospace GmbH and Co. KG, Schweinfurt, Germany

References

[1] Voskamp AP. Material response to rolling contact loading. ASME Journal of Tribology. 1985;**107**(3):359-367

[2] Beer O. Structural changes induced by rolling contact fatigue – Results from rig testing and field experience. HTM Journal of Heat Treatment and Materials. 2017;**72**(4):205-214

[3] Beer O, Fella J. Untersuchung struktureller Veränderungen durch Überrollbeanspruchung mittels röntgenografischer Methoden. HTM Journal of Heat Treatment and Materials. 2015;**70**(3):142-149

[4] Böhmer HJ, Hirsch Th. Der Einsatz von Eigenspannungsmessungen zur Bewertung des Wälzermüdungsverhaltens von Werkstoffen. In: Bauteilversagen durch Mikrodefekte, DVM-Bericht 518; 1998. pp. 27-47

[5] Gegner J, Nierlich W. Comparison of microstructural changes and X-ray diffraction peak width decrease during rolling contact fatigue in martensitic microstructures. In: Advances in Rolling Contact Fatigue Strength Testing and Related Substitute Technologies, STP 1548 Int. Conshohocken, PA, USA; 2012. pp. 303-328

[6] Noyan IC, Cohen JB. Residual Stress Measurement by Diffraction and Interpretation. Berlin: Springer; 1987

[7] Böhmer, internal communication

[8] Hill DA, Ashelby DW. The influence of residual stresses on contact load bearing capacity. Wear. 1982;**75**(2):221-240

[9] Broszeit E, Adelmann J, Zwirlein O. Einfluß von Eigenspannungen auf die Werkstoffanstrengung in wälzbeanspruchten Bauteilen. Materialwissenschaft und Werkstofftechnik. 1985;**16**(1):19-24

IntechOpen

IntechOpen